The crystal structure of ammoniojarosite, (NH₄)Fe₃(SO₄)₂(OH)₆ and the crystal chemistry of the ammoniojarosite−hydronium jarosite solid-solution series

L. C. Basciano* and R. C. Peterson

Department of Geological Sciences and Geological Engineering, Queen's University, Kingston, Ontario, Canada, K7L 3N6

ABSTRACT

The atomic structure of ammoniojarosite, [(NH₄)Fe₃(SO₄)₂(OH)₆], a = 7.3177(3) Å, c = 17.534(1) Å, space group $R\bar{3}m$, Z = 3, has been solved using single-crystal X-ray diffraction (XRD) to wR 3.64% and R 1.4%. The atomic coordinates of the hydrogen atoms of the NH₄ group were located and it was found that the ammonium group has two different orientations with equal probability. Hydronium commonly substitutes into jarosite group mineral structures and samples in the ammoniojarosite−hydronium jarosite solid-solution series were synthesized and analysed using powder XRD and Rietveld refinement. Changes in unit-cell dimensions and bond lengths are noted across the solid-solution series. The end-member ammoniojarosite synthesized in this study has no hydronium substitution in the A site and the unit-cell dimensions determined have a smaller a dimension and larger c dimension than previous studies. Two natural ammoniojarosite samples were analysed and shown to have similar unit-cell dimensions to the synthetic samples. Short-wave infrared and Fourier transform infrared spectra were collected for samples from the NH₄–H₃O jarosite solid-solution series and the differences between the end-members were significant. Both are useful tools for determining NH₄ content in jarosite group minerals.

Introduction

Ammoniojarosite has been studied extensively as it is a by-product of the zinc industry (Salinas *et al*., 2001), where it is used to precipitate dissolved Fe from the hot acid leach solutions prior to zinc recovery. One hundred and twenty-five thousand tonnes of jarosite containing 25−36 wt.% Fe is produced annually (Dutrizac and Jambor, 2000). Ammoniojarosite and sodium jarosite are less expensive and hence more commonly used. Natural ammoniojarosite is rare because concentrated ammonium-containing solutions are not common − the ammonium itself must come from

the decomposition of organic substances or biological activity associated with organic matter (Frost *et al*., 2006). Natural ammoniojarosite is most often found in lignitic shale associated with other ammonium-bearing minerals. Natural ammoniojarosite has been reported in samples from Buffalo, Wyoming (Odem *et al*., 1982) and southern Utah (Shannon, 1927, 1929).

Ammonioalunite (NH₄)Al₃(SO₄)₂(OH)₆ was first described by Altaner *et al*. (1988) in a sample from the hot springs at The Geysers (Sonoma County), California. The ammonio-alunite was intermixed with ammoniojarosite. In that same study, ammonioalunites with intermediate NH₄⁺ substitution were described from the Ivanhoe Deposit (Elko County), California. The

* E-mail: basciano@students.geol.queensu.ca

ammonioalunite from The Geysers forms in NH_4-rich fluids and the ammonioalunite samples from the Ivanhoe deposit form in hydrothermally altered basalt (Altaner *et al.*, 1988). The rarity of ammonioalunite is attributed to the different environments of formation and occurrence of aqueous NH_4^+ and alunite-group minerals, with the former most abundant in reducing and acidic fluids, while the latter forms in oxidizing and acidic environments. Similar to ammoniojarosite, ammonioalunite requires fluids with a small K content, as K will readily substitute into the structure in preference to NH_4.

The jarosite group of minerals is part of the alunite supergroup, which consists of 40 mineral species that have the general formula $AB_3(TO_4)_2(OH)_6$. There is extensive solid solution in the *A*, *B* and *T* sites within the alunite supergroup, where *A* is H_3O^+, Na^+, K^+, Rb^+, Ag^+, Tl^+, NH_4^+, $0.5Ca^{2+}$ or $0.5Pb^{2+}$, *B* is Fe^{3+} or Al^{3+} and TO_4 is SO_4^{2-}, PO_4^{3-} or AsO_4^{3-} (Scott, 1987; Stoffregen and Alpers, 1987). The jarosite group is characterized by $B = Fe^{3+}$ and $T = S$. Jarosite (*A* = K) and natrojarosite (*A* = Na) are the most prevalent naturally occurring jarosite-group minerals. End-member hydronium jarosite is rare, although most jarosite group minerals contain some hydronium in the *A* site (Ripmeester *et al.*, 1986; Drouet and Navrotsky, 2003; Majzlan *et al.*, 2004; Basciano and Peterson, 2007).

The unit-cell dimensions were determined for synthetic ammoniojarosite samples by Smith and Lampert (1973) and Dutrizac and Kaiman (1976). Neither sample was end-member ammoniojarosite and both exhibited significant H_3O substitution in the *A* site.

Natural and synthetic jarosite group minerals commonly have significant quantities of hydronium in the alkali (*A*) site and minor to major deficiencies in the Fe site (*B*). Most jarosite-group minerals synthesized in previous studies and many natural jarosite group minerals have *B* site occupancies as low as 86%. Studies that address the Fe and/or Al deficiency are: Hendricks (1937), Kubisz (1970), Ripmeester *et al.* (1986), Drouet and Navrotsky (2003) and Drouet *et al.* (2004).

The crystal structure, including hydrogen positions of the OH and NH_4 groups, was determined in this study using single-crystal XRD. In addition, structures were refined using Rietveld refinement of ammoniojarosite and three samples in the ammoniojarosite−hydronium jarosite solid-solution series. Two natural samples of ammoniojarosite were analysed and compared to the synthetic samples. Short wave infrared (SWIR) spectra and Fourier transform infrared (FTIR) spectra were collected from the synthetic samples to determine the changes in the IR spectra due to H_3O content.

Materials and methods

Natural samples

Two natural samples were obtained from the Royal Ontario Museum in Toronto, Canada, for analysis. Sample M38446 is from Buffalo, Johnson County, Wyoming. The sample locality was originally described by Odem *et al.* (1982). The specimen itself is fine-grained, yellow and occurs as aggregates; the ammoniojarosite was found in a lignitic black to brown shale (Odem *et al.*, 1982). Sample M16514 is from the west side of the Kaibab Fault, southern Utah. The sample and its associated area were originally described by Shannon (1927, 1929). Shannon (1927) described M16514 as small lumps and hard irregular flattened nodules up to 4 cm wide by 5 mm thick, embedded in blackish-brown lignitic material. The ammoniojarosite is closely associated with tschermigite ($NH_4Al(SO_4)_2.12H_2O$). The two natural samples were analysed using powder XRD to determine unit-cell dimensions and with scanning electron microscopy − energy dispersive spectroscopy (SEM-EDS) to determine if there were any chemical substitutions in the *A* or *B* sites, which would affect the unit-cell dimensions.

Synthetic samples

The solid-solution series (H_3O,NH_4) $Fe_3(SO_4)_2(OH)_6$ was synthesized using conditions outlined in Basciano and Peterson (2007) to ensure full Fe occupancy in the samples. Forty grams of reagent-grade $Fe_2(SO_4)_3.5H_2O$ and varying amounts of reagent-grade $(NH_4)_2SO_4$ (0.2, 0.4 and 1.0 g) were mixed with de-ionized water to a volume of 100 ml at room temperature and heated in sealed stainless-steel bombs at 140ºC for 48 h. During the $H_3O−NH_4$ jarosite solid-solution synthesis, ammonium-rich jarosite precipitated out of solution first in all samples, followed by hydronium-rich jarosite. Ammoniojarosite may have a lower solubility product than hydronium jarosite, causing it to precipitate out of solution first as in the case with Na and K jarosite (Glynn, 2000). The chemical compositions of the starting solutions

and the analytical results of the resulting ammoniojarosite–hydronium jarosite samples are given in Table 1. X-ray diffraction scans of samples B, C and D show that a number of the peaks are broadened due to the heterogeneity of the samples. As ammoniojarosite preferentially precipitates out of solution before hydronium-rich jarosite, the samples are composed of a combined chemistry along the solid-solution series. The peak-broadening was most evident for peak 006 where there is a large difference in position between ammonium-rich and ammonium-poor phases in the mixture. Similar findings are discussed in Basciano and Peterson (2007) for the potassium−hydronium jarosite solid-solution series. To produce a single homogeneous phase, the samples were finely ground in a McCrone Micronizing Mill after the initial synthesis and re-heated at 140ºC in the reactant solution. Samples were analysed every three days using XRD to determine sample homogeneity. The samples were deemed to be homogeneous when the full width at half maximum (FWHM) of peak 006 did not decrease with further annealing. All samples were rinsed thoroughly with de-ionized water, filtered and dried at 120ºC to eliminate any excess water. Drying at this temperature did not influence the XRD pattern of the samples. All samples consisted of intergrown rhombohedral (pseudocubic) crystals varying in size from <10 μm (initial growth) to 100 μm (final growth). Data for end-member hydronium jarosite was taken from Basciano and Peterson (2007). End-member ammoniojarosite could not be grown using the above method as there was hydronium substitution in the A site in all samples as determined by Rietveld refinement and analysis of unit-cell dimensions.

End-member ammoniojarosite was grown using a two-step method similar to Stoffregen (1993). Ammoniojarosite with ~80% NH_4 occupancy was grown using the same method outlined above. To produce single-crystals and a powder for Rietveld refinement the resulting sample was heated in a 1.0 M H_2SO_4-0.5NH_4SO_4 solution at 200ºC for 3 days in a Parr pressure bomb. This procedure yielded a sample with A site occupancy of 100% NH_4 as determined by inductively coupled plasma optical emission spectroscopy (ICP-OES) and inductively coupled plasma mass spectrometry (ICP-MS). Crystals were hand-picked from the bulk material for single-crystal analysis and the remainder of the sample was ground in a McCrone Micronising Mill for powder XRD and Rietveld refinement.

Diffraction experiments

Single-crystal XRD

A single-crystal of end-member ammoniojarosite (amber coloured, cubic shaped, $0.10 \times 0.08 \times 0.06$ mm) was mounted on a glass fibre for XRD analysis. Data collection was performed using a Bruker SMART CCD 1000 X-ray diffractometer with a graphite-monochromated Mo-$K\alpha$ radiation ($\lambda = 0.71073$ Å), operating at 50 kV and 35 mA at 180 K over a 2θ range of 3.42 to 28.08º (Department of Chemistry, Queen's University). Data were processed using the Bruker AXS Crystal Structure Analysis Package. The single-crystal unit-cell dimensions were obtained using *APEX2* and refined with *SAINT* software, using all observed reflections. The raw intensity data were converted (including corrections for background, Lorentz and polarization effects) to

TABLE 1. Chemical compositions of starting solutions and synthetic jarosite samples.

Synthetic samples	Starting solution compositions (g)		Analytical results − ICP-OES and ICP-MS Formula
	$(NH_4)_2(SO_4)$	$Fe_2(SO_4)_2 \cdot xH_2O$	
A*	0.0	40	$(H_3O)Fe_{3.06}(SO_4)_2(OH)_6$
B	0.2	40	$[(NH_4)_{0.32}(H_3O)_{0.68}]Fe_{3.04}(SO_4)_2(OH)_6$
C	0.4	40	$[(NH_4)_{0.59}(H_3O)_{0.39}]Fe_{3.03}(SO_4)_2(OH)_6$
D	1.0	40	$[(NH_4)_{0.93}(H_3O)_{0.07}]Fe_{3.05}(SO_4)_2(OH)_6$
E[†]			$(NH_4)_{1.08}Fe_{3.10}(SO_4)_2(OH)_6$

* From Basciano and Peterson (2007)

[†] See text for sample synthesis

TABLE 2. Ammoniojarosite: data collection and structure refinement information for single-crystal data.

IGG identification code	
Wavelength (Å)	0.71073
Crystal system	Hexagonal
Space group	$R\bar{3}m$
Unit-cell dimensions (Å)	$a = 7.3177(3)$
	$c = 17.534(1)$
Volume (Å^3)	813.15(8)
Z	3
Absorption coefficient (mm^{-1})	4.433
θ range for data collection (º)	3.42 to 28.08
Index ranges	$-9 \leqslant h \leqslant 9$
	$-9 \leqslant k \leqslant 9$
	$-22 \leqslant l \leqslant 22$
Reflections collected	2978
Independent reflections	276
R(int)	0.0141
Completeness to θ = 28.08º	98.6%
Data/restraints/dimensions	276/1/32
Data fit quality on F^2	1.242
Final R indices ($I>2\sigma(I)$)	$R1 = 0.0140$
	$wR2 = 0.0364$
R indices (all data)	$R1 = 0.0145$
	$wR2 = 0.068$

structure amplitudes and their respective estimated standard deviation values using the *SAINT* program. Structure solution was carried out using *XPREP* and *SHELXTL* (Bruker, 2000), the structure refinement was also performed with *SHELXTL*. The X-ray single-crystal data set includes 2978 reflections, which sorted to 276

unique reflections with an agreement factor of $R = 0.014$ in space group $R\bar{3}m$. Scattering curves for neutral atoms were taken from the *International Tables for X-ray Crystallography, Vol. C*. Least-squares refinement including anisotropic temp-erature factors and site-occupancy factors, with disordered H atoms, resulted in a wR of 0.04. Hydrogen atoms which are part of the NH$_4$ group were soft constrained so that bond distances N$-$H2 and H3 were approximately equal and the atomic displacement parameters of H1, H2 and H3 were restrained to be equal. The Fo-Fc tables are deposited as supplementary data with the Principle Editor and can be found at http://www.minersoc.org/pages/e_journals/dep_mat.html. Data collection and structure refinement details are given in Table 2, atomic coordinates and temperature factors are given in Table 3, while bond lengths and angles can be found in Table 4.

Powder XRD and Rietveld refinement

Powder XRD data were collected from 15$-$100º2θ (Fe filtered Co-$K\alpha$ radiation) from a back-packed sample using a Panalytical X'Pert theta-theta diffractometer and an X'celerator position-sensitive detector equipped with incident- and diffracted-beam soller slits, with 0.5º diver-gence and 1º anti-scatter slits. The normal-focus Co X-ray tube was operated at 40 kV and 45 mA. Profiles were taken with a step interval of 0.008º2θ and an equivalent counting time per step of 30 s. To eliminate preferred orientation, samples were ground for 2 min in a McCrone Micronizing Mill and backpacked on 320 grit sandpaper. The data were refined with the Rietveld refinement program

TABLE 3. Atom coordinates and anisotropic-displacement dimensions (Å$^2 \times 10^3$) for ammoniojarosite, determined by single-crystal refinement.

Atom	Position	x	y	z	U_{eq}	U_{11}	U_{22}	U_{33}	U_{23}	U_{13}	U_{12}
Fe	9d	0.1667	−0.1667	−0.1667	6(1)	5(1)	5(1)	8(1)	0(1)	0(1)	3(1)
S	6c	0	0	0.3059(1)	6(1)	6(1)	6(1)	6(1)	0	0	3(1)
O1	6c	0	0	0.3891(1)	9(1)	11(1)	11(1)	7(1)	0	0	5(1)
O2	18h	0.2231(1)	−0.2231(1)	−0.0564(1)	9(1)	11(1)	11(1)	9(1)	0(1)	0(1)	8(1)
O3	18h	0.1277(1)	−0.1277(1)	0.1371(1)	8(1)	6(1)	6(1)	11(1)	−1(1)	1(1)	3(1)
N	3a	0	0	0	10(1)	12(1)	12(1)	7(2)	0	0	6(1)
H1	18h	0.176(2)	−0.176(2)	0.118(2)	27(8)	−	−	−	−	−	−
H2	18h	0.059(3)	0.119(6)	0.018(3)	27(8)	−	−	−	−	−	−
H3	6c	0	0	−0.047(2)	27(8)	−	−	−	−	−	−

The anisotropic displacement factor takes the form: $-2\pi^2[h^2a^{*2}U^{11}+\cdots+2hka^*b^*U^{12}]$

TABLE 4. Selected interatomic distances (Å) and angles (°) for ammoniojarosite, as determined by single-crystal diffraction.

$Fe-O3 \times 4$	1.9832 (6)	$O3-H1$	0.70(2)
$Fe-O2 \times 2$	2.062 (1)	$H2 \cdots O3$	2.25(4)
Average	2.009		
		$O2-Fe-O3 \times 4$	89.00(5)
$S-O1$	1.459 (2)	$O2-Fe-O3 \times 4$	91.00(5)
$S-O2 \times 3$	1.486 (1)	$O3-Fe-O3 \times 2$	89.98(8)
Average	1.479	$O3-Fe-O3 \times 2$	90.02(8)
$N-O3$	2.898 (1)	$O1-S-O2 \times 3$	109.97(6)
$N-O2$	2.9957 (8)	$O2-S-O2 \times 3$	108.97(6)
		Average	109.47
$N-H2$	0.82 (3)		
$N-H3$	0.82 (4)	$H2-N-H3$	113(4)

Symmetry transformations used to generate equivalent atoms:
(1) $x-y,x,-z$
(2) $y,-x+y,-z$
(3) $-x+y+1/3,-x-1/3,z-1/3$
(4) $-y+1/3,x-y-1/3,z-1/3$
(5) $-x+1/3,-y-1/3,-z-1/3$
(6) $-y-1/3,x-y-2/3,z+1/3$
(7) $-x+y+2/3,-x+1/3,z+1/3$
(8) $x-1/3,y+1/3,z+1/3$
(9) $x+1/3,y-1/3,z-1/3$
(10) $x,x-y,z$

Topas Academic (Coelho, 2004). Initial atomic positions were taken from the single-crystal results of this study. The instrument dimensions were modelled using a full axial divergence model as defined by Cheary and Coelho (1998) and the Co-$K\alpha$ source emission profiles were taken from Hölzer *et al.* (1997). Broadening due to crystallite size was refined using the Double-Voigt approach (Balzar, 1999).

The nitrogen of the NH_4 group was located at (0,0,0) similar to the oxygen of the hydronium jarosite (Majzlan *et al.*, 2004; Basciano and Peterson, 2007). The occupancy of ammonium in the *A* site was fixed to the occupancy determined using ICP-OES and ICP-MS and the *T* site is assumed to be fully occupied by S. The starting hydrogen positions (OH group) were taken from the single-crystal study of hydronium jarosite by Majzlan *et al.* (2004) and the starting hydrogen positions (NH_4 group) were taken from single-crystal results (this study). Without restraint, the O−H1 bond lengths for the OH group were significantly shorter than typical values. The O−H1 bond lengths were restrained to 0.8 Å, which is the average O−H bond length in crystalline solids refined by XRD (Baur, 1972). Observed O−H distances in X-ray determinations tend to be, on average, 0.2 Å shorter than in neutron diffraction (Baur, 1972). The atomic displacement parameters of the H atoms were fixed at 2 and unrefined. The atomic position of H2 and H3 (NH_4 group) were not refined due to the two possible orientations of the NH_4 group and low scatter of H with occupancy of H_3O in the *A* site. Isotropic displacement parameters (B) for N, Fe, S and O were refined with no restrictions and were found to be low for O3. The *z* coordinate of H1 for samples B, C and D (samples intermediate between hydronium jarosite and ammoniojarosite) are probably inaccurate and indicate a systematic error in the refinement. A final Rietveld refinement plot of observed and calculated intensities for end-member ammoniojarosite is shown in Fig. 1.

Chemical analysis

The Fe and S contents of the solid jarosite samples were determined using a Varian vista CCD Simultaneous ICP-OES at the Analytical Services Unit of Queen's University. The solid samples were digested in aqua regia and both these and reactant solutions were diluted for analysis. The average analytical errors for Fe and
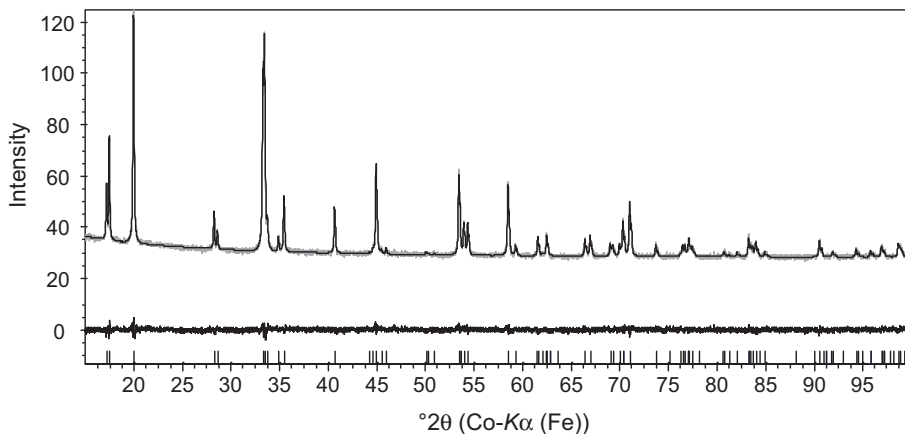
FIG. 1. Rietveld refinement plot of sample E, ammoniojarosite. The grey line represents the observed data and the solid line the calculated pattern. The vertical bars mark all possible Bragg reflections (Co-$K\alpha_1$ and $K\alpha_2$). The difference between the observed and calculated patterns is shown at the bottom.

S are ±1% and ±2%, respectively. The N content of the solid jarosite phases were determined using a Costech Elemental Analyser coupled to a Thermo Finnigan Delta plus XP using continuous flow technology. The average analytical error for N is ±2%. From these data the stoichiometry of the ammonium group and Fe site were determined in the solid samples, based on the ratio of N and Fe to S. The percentages of N and Fe in these sites were normalized to 2 S per chemical formula based on the ideal chemical formula. The chemical compositions of the synthetic samples

are given in Table 1. The A site is assumed to be full and to contain H_3O.

Short-wave infrared reflectance spectroscopy and Fourier transform infrared analysis

Short-wave infrared reflectance spectra of the synthetic samples were collected using a portable infrared mineral analyser, an Integrated Spectronics PIMA SP instrument, in the 1200−2600 nm range. Infrared spectra of the synthetic samples were collected using a Nicolet
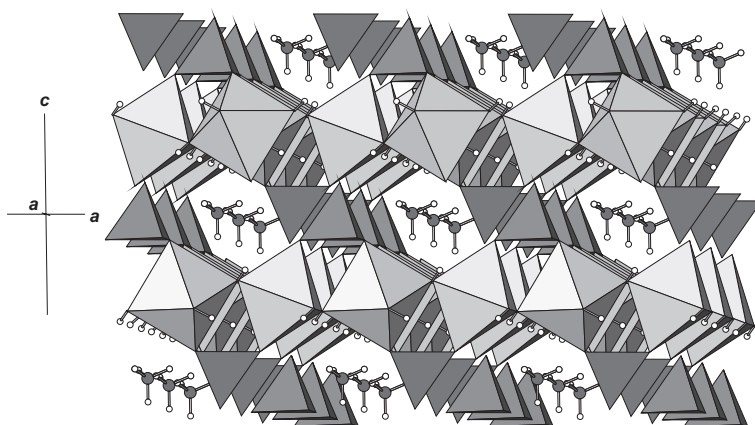

FIG. 2. Polyhedral representation of the ammoniojarosite structure (*ATOMS* 6.0, Dowty, 2003). Sulphate tetrahedra are dark grey, Fe octahedra are light grey, N atoms are dark grey spheres and positionally disordered H atoms are white spheres.

Avatar 320 Fourier transform infrared spectrometer and attenuated total reflectance spectra were measured, using a Golden Gate diamond ATR spectrometer, in the range $400-4000$ cm^{-1}. The samples were analysed by SWIR and IR as finely ground powders after being micronized for Rietveld refinement.

Discussion

Description of the structure of ammoniojarosite

The structure of ammoniojarosite was determined using single-crystal XRD at 180 K. A structure diagram of ammoniojarosite is shown in Fig. 2 (one orientation of NH$_4$ shown). Members of the jarosite group crystallize in space group $R\bar{3}m$, with $Z = 3$ (in the hexagonal unit cell). The basic structure of the jarosite group consists of SO$_4$ tetrahedra and Fe-cation octahedra, where the octahedra corner-share to form sheets perpendicular to the c axis. Two different orientations of SO$_4$ tetrahedra occur within a layer; one set pointing towards $+c$ alternates with another set pointing towards $-c$. The oxygen and hydroxyl
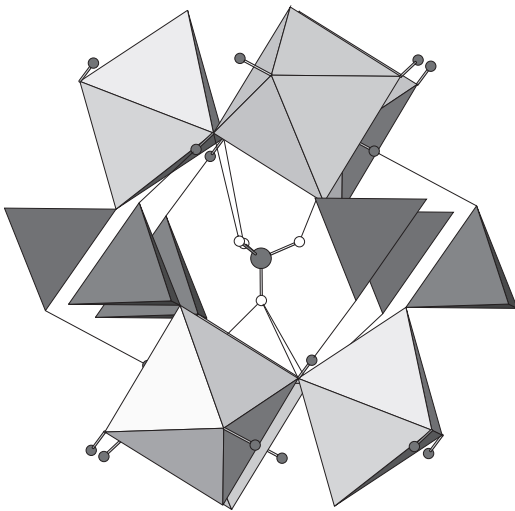
FIG. 3. Polyhedral drawing showing the hydrogen bonding scheme of the ammonium groups in the A site of ammoniojarosite (*ATOMS* 6.0, Dowty, 2003). Only one orientation of the ammonium group is shown for clarity. Iron octahedra are shown in light grey and sulphate tetrahedra are dark grey. The N atom is shown in dark grey; H1 atoms are small dark grey spheres; H2 and H3 are small white spheres (bonded to N). Hydrogen bonding is shown as thin lines.

groups form an icosahedron, in which the alkali cation, hydronium or ammonium group is located. The univalent cations (K$^+$, H$_3$O$^+$, NH$_4^+$, etc) are surrounded by twelve anions, consisting of six oxygen atoms (O2) and six OH groups (O3).

The ammonium group is disordered and has two orientations with equal probability. The hydrogen bonding scheme of one orientation of the NH$_4$ group is shown in Fig. 3. Nitrogen is located at special position 3a (0, 0, 0) and is coordinated by four hydrogen atoms forming a tetrahedron. The N−H2 and N−H3 distances are 0.82 Å and the H2−N−H3 angle is 113°. The

TABLE 5. Calculated powder diffraction pattern of synthetic ammoniojarosite ($I/I_o \geqslant 3$; the ten strongest reflections are in bold).

I/I_o	°2θ	$d_{(calc)}$ (Å)	No.*	h k l
13.5	**17.25**	**5.963**	**6**	**1 0 1**
30.5	**17.53**	**5.870**	**2**	**0 0 3**
100.0	**20.03**	**5.144**	**6**	**0 1 2**
9.3	28.30	3.659	6	1 1 0
3.9	28.65	3.616	6	1 0 4
74.5	**33.34**	**3.119**	**6**	**0 2 1**
95.0	**33.49**	**3.105**	**12**	**1 1 3**
5.5	33.78	3.078	6	0 1 5
3.4	34.92	2.982	6	2 0 2
16.1	**35.49**	**2.935**	**2**	**0 0 6**
12.9	40.71	2.572	6	0 2 4
32.5	**44.99**	**2.338**	**6**	**1 0 7**
28.9	**53.49**	**1.988**	**6**	**0 3 3**
9.2	54.00	1.970	6	0 2 7
9.3	54.41	1.957	2	0 0 9
26.5	**58.54**	**1.829**	**6**	**2 2 0**
5.3	61.61	1.747	12	2 2 3
6.1	62.52	1.724	12	3 1 2
4.9	66.46	1.632	12	1 3 4
6.2	66.99	1.621	12	1 2 8
3.8	69.06	1.578	6	4 0 1
3.5	70.01	1.559	6	0 4 2
11.8	70.36	1.553	12	2 2 6
21.0	**71.06**	**1.539**	**6**	**0 2 10**
3.7	73.74	1.491	6	4 0 4
3.3	76.50	1.445	6	0 4 5
4.8	77.15	1.434	12	2 3 2
3.9	83.29	1.346	12	4 1 3
4.6	84.04	1.336	12	2 2 9
6.4	90.57	1.259	12	3 2 7
3.1	94.35	1.220	6	3 3 0
3.2	96.94	1.195	12	2 4 1
4.8	98.69	1.179	12	2 1 13
3.0	98.83	1.178	6	4 0 10

* Reflection multiplicity

TABLE 6. Data collection and structure-refinement details: Rietveld refinement of powder diffraction data.

Ammoniojarosite−hydronium jarosite $R\bar{3}m$

Sample	E	D	C	B	A
NH$_4$ (%)	100	93	59	32	0*
a (Å)	7.31780 (8)	7.3226 (1)	7.3293 (2)	7.3431 (1)	7.3552 (2)
c (Å)	17.6094 (2)	17.4990 (3)	17.3584 (4)	17.1595 (4)	16.9945 (4)
V (Å^3)	816.65 (2)	812.60 (2)	807.54 (4)	801.30 (4)	796.21 (4)
R_p	2.744	5.689	6.104	7.165	3.571
R_{wp}	3.500	8.025	9.348	11.427	4.773
R_{exp}	3.104	4.811	4.349	4.457	3.882
S	1.128	1.668	2.150	2.564	1.230
D−W	0.848	0.383	0.238	0.174	0.691

R_p: R-pattern, R_{wp}: weighted-pattern, R_{exp}: R-expected, S (= R_{wp}/R_{exp}): quality of fit (Young, 1993)
D−W: Durbin-Watson d statistic (Hill and Flack, 1987)
* From Basciano and Peterson (2007)

average N−H bond length, based on neutron diffraction studies of many compounds, is 1.01 Å, with a range of 0.94−1.10 Å and an average H−N−H angle of 110º with a range of 104−122º (Baur, 1972). The observed N−H bond length is shorter than the average determined from neutron diffraction because hydrogen bond lengths tend to be shorter in structures determined using XRD. It

was found by Baur (1972) that observed O−H distances in X-ray determinations tend to be on average 0.2 Å shorter than neutron diffraction. The H2−N−H3 angle of 113º is very close to the average H−N−H angle (º). The N−H···O3 distance is 2.898 Å and H···O3 distance is 2.26 Å. The remainder of the structure is similar to the other members of the jarosite group.
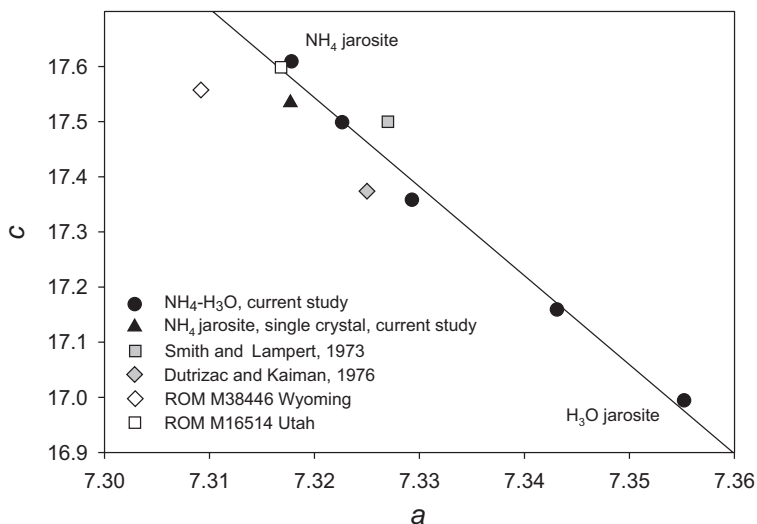

FIG. 4. Unit-cell parameters c vs. a of synthetic NH$_4$−H$_3$O solid-solution series from the current study, synthetic samples from previous studies and natural ammoniojarosite samples. Samples from the current synthetic powder diffraction study are shown as black circles, samples from previous studies are shown in grey and natural samples are shown in white. Note that the unit-cell dimension of ammoniojarosite from this study (far left sample, black circle) has a smaller a dimension and a larger c dimension than previously synthesized ammoniojarosite. This is because there is no hydronium substitution in the A site. If any of the samples had Fe deficiencies in the B site, the cell dimensions would have smaller c cell parameters than the samples synthesized in this study.

TABLE 7. Refined atomic positions, displacement parameters and occupancies of synthetic ammoniojarosite–hydronium jarosite samples as determined by powder XRD and Rietveld refinement.

Site	W	x	y	z	B (Å^2)	Occupancy
Sample A*						
H$_3$O	3a	0	0	0	3.4 (5)	0.92 (1)
Fe	9d	0.16667	−0.16667	−0.16667	1.99 (8)	1
S	6c	0	0	0.3095 (2)	0.9 (1)	1
O1	6c	0	0	0.3946 (3)	2.6 (3)	1
O2	18h	0.2253 (3)	−0.2253 (3)	−0.0565 (2)	1.5 (2)	1
O3	18h	0.1279 (2)	−0.1279 (2)	0.1368 (1)	0.5 (1)	1
H1	18h	0.163 (1)	−0.163 (1)	0.100 (1)	2	1
Sample B						
N	3a	0	0	0	7.4 (5)	0.32
H$_3$O	3a	0	0	0	7.4 (5)	0.68
Fe	9d	0.16667	−0.16667	−0.16667	3.12 (9)	1
S	6c	0	0	0.3088 (3)	1.6 (1)	1
O1	6c	0	0	0.3969 (6)	5.8 (4)	1
O2	18h	0.2268 (3)	−0.2268 (3)	−0.0582 (3)	2.3 (2)	1
O3	18h	0.1283 (2)	−0.1283 (2)	0.1363 (2)	0.3 (2)	1
H1	18h	0.170 (2)	−0.170 (2)	0.168 (2)	2	1
H2[†]	6c	0.059	0.119	0.018	2	0.16
H3[†]	6c	0	0	−0.047	2	0.16
Sample C						
N	3a	0	0	0	3.3 (4)	0.59
H$_3$O	3a	0	0	0	3.3 (4)	0.41
Fe	9d	0.16667	−0.16667	−0.16667	2.19 (6)	1
S	6c	0	0	0.3065 (2)	1.12 (9)	1
O1	6c	0	0	0.3923 (4)	3.2 (3)	1
O2	18h	0.2259 (2)	−0.2259 (2)	−0.0577 (2)	1.4 (1)	1
O3	18h	0.1291 (2)	−0.1291 (2)	0.1355 (2)	0.2 (2)	1
H1	18h	0.152 (1)	−0.152 (1)	0.176 (2)	2	1
H2[†]	6c	0.059	0.119	0.018	2	0.30
H3[†]	6c	0	0	−0.047	2	0.30
Sample D						
N	3a	0	0	0	1.5 (3)	0.93
H$_3$O	3a	0	0	0	1.5 (3)	0.07
Fe	9d	0.16667	−0.1667	−0.16667	1.65 (5)	1
S	6c	0	0	0.3070 (2)	0.96 (8)	1
O1	6c	0	0	0.3920 (3)	1.2 (2)	1
O2	18h	0.2244 (2)	−0.2244 (2)	−0.0573 (2)	0.7 (1)	1
O3	18h	0.1309 (2)	−0.1309 (2)	0.1349 (2)	0.3 (1)	1
H1	18h	0.130 (2)	−0.130 (2)	0.178 (1)	2	1
H2[†]	6c	0.059	0.119	0.018	2	0.47
H3[†]	6c	0	0	−0.047	2	0.47
Sample E						
N	3a	0	0	0	4.2 (3)	1
H$_3$O	3a	0	0	0	4.2 (3)	0
Fe	9d	0.16667	−0.16667	−0.16667	1.40 (4)	1
S	6c	0	0	0.3051 (1)	0.34 (8)	1
O1	6c	0	0	0.3897 (2)	0.5 (1)	1
O2	18h	0.2235 (2)	−0.2235 (2)	−0.0571 (1)	0.1 (1)	1
O3	18h	0.12743 (9)	−0.12743 (9)	0.1376 (1)	0.07 (9)	1
H1	18h	0.1899 (9)	−0.1899 (9)	0.129 (1)	2	1
H2[†]	6c	0.059	0.119	0.018	2	0.5
H3[†]	6c	0	0	−0.047	2	0.5

* Data taken from Basciano and Peterson (2007)
[†] Atomic positions taken from single-crystal results, current study.
Numbers in parentheses in this and subsequent tables are estimated standard deviations.

As part of the ammoniojarosite−hydronium jarosite solid-solution study the structure of end-member ammoniojarosite was refined using powder XRD data collected at room temperature with Rietveld refinement. Unit-cell dimension a of both sets of data are very similar (single-crystal a: 7.3177 Å, powder a: 7.3178 Å). Unit-cell dimension c of the powder data is 0.074 Å larger than the single-crystal data (single-crystal c: 17.534 Å, powder c: 17.609 Å). This can be attributed to the temperature difference during data collection, with the single-crystal data collected at liquid nitrogen temperature and the powder data collected at room temperature. These results show that at these temperatures any increase mainly affects cell dimension c and not a. The increase in temperature causes a lengthening of the bonds N−H···O2 and N−H···O3 by 0.010 and 0.014 Å, respectively. The N−H···O3 bond is largely along the c axis and N−H···O2 has a component along the c axis. As the unit-cell dimension of ammoniojarosite is much larger along c than a, changes in bond length parameters affect the c dimension to a greater degree. In addition, the ammoniojarosite structure is more weakly bonded in the c dimension because the linking along the c axis is related to the hydrogen bonding of O1···H1−O3 and the bifurcated hydrogen bond with H in the disordered NH_4^+ groups with O2 and O3 anions. These bonds produce a larger allowance in the c direction than rotation of the Fe octahedra or dilation of the Fe−O bonds along a.

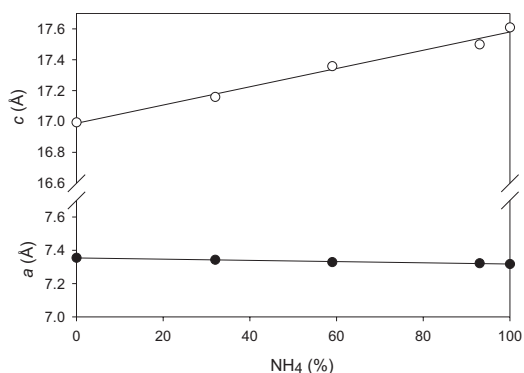The calculated intensities and positions of diffraction peaks for synthetic ammoniojarosite are listed in Table 5. These represent an improvement on previous published diffraction patterns (Dutrizac and Kaiman, 1976; Smith and Lampert, 1973) as a result of the full occupancy of NH_4 in the A site, with no H_3O substitution. In reference pattern 026−1014 (Smith and Lampert, 1973) of the International Centre for Diffraction Data database (PDF-2 database, 2001) there are several peaks which are shifted due to the hydronium content, whereas others were simply measured as one peak, where in the current study, two or more exist.

Solid-solution and structural dimensions

As hydronium is very common in the jarosite group of minerals and readily substitutes in the A site of natural and synthetic ammoniojarosite, the ammoniojarosite−hydronium jarosite series was examined using powder XRD and Rietveld
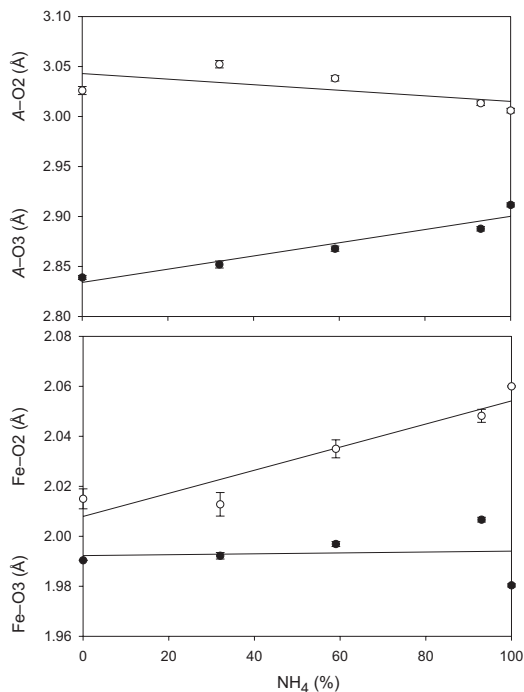

FIG. 6. A−O polyhedral bond lengths and Fe−O octahedral bond lengths *vs.* A site occupancy in the ammoniojarosite−hydronium jarosite solid-solution series. Polyhedral bond lengths of the A and B sites vary linearly with NH_4 occupancy in the A site. The A−O2 bond length for hydronium jarosite is smaller than the trend would indicate due to non-stoichiometry of the A site with 92% H_3O occupancy (Basciano and Peterson, 2007).

FIG. 5. Unit-cell dimensions a and c *vs.* ammonium occupancy in the A site. Increased NH_4 content leads to a larger c unit-cell parameter. Error bars reported by Rietveld refinement are smaller than the symbols.

TABLE 8. Selected interatomic distances (Å) and angles (°) of ammoniojarosite−hydronium jarosite solid-solution samples as determined by powder XRD and Rietveld refinement.

A-site occ. (%NH$_4$)	E 100	D 93	C 59	B 32	A* 0
A−O3 × 6	2.912 (2)	2.886 (2)	2.868 (3)	2.852 (3)	2.839 (2)
A−O2 × 6	3.006 (2)	3.017 (2)	3.038 (3)	3.052 (4)	3.026 (4)
Average	2.959	2.951	2.953	2.952	2.932
Fe−O3 × 4	1.9804 (6)	2.0062 (9)	1.997 (1)	1.992 (1)	1.9904 (9)
Fe−O2 × 2	2.060 (2)	2.049 (3)	2.035 (4)	2.013 (5)	2.015 (4)
Average	2.007	2.020	2.010	1.999	1.999
S−O1	1.490 (4)	1.486 (6)	1.491 (8)	1.51 (1)	1.447 (7)
S−O2 × 3	1.482 (2)	1.484 (3)	1.465 (3)	1.473 (4)	1.485 (4)
Average	1.484	1.484	1.471	1.482	1.476
O2−Fe−O3 × 4	89.32 (7)	88.28 (7)	89.35 (9)	89.6 (1)	89.6 (1)
O2−Fe−O3 × 4	90.68 (7)	91.72 (7)	90.65 (9)	90.4 (1)	90.4 (1)
O3−Fe−O3 × 2	89.87 (7)	88.4 (1)	89.4 (1)	89.6 (2)	89.7 (1)
O3−Fe−O3 × 2	90.13 (7)	91.6 (1)	90.6 (1)	90.4 (2)	90.3 (1)
O1−S−O2 × 3	110.03 (9)	111.4 (2)	111.5 (2)	113.1 (2)	112.0 (1)
O2−S−O2 × 3	108.91 (9)	107.4 (2)	107.4 (2)	105.6 (2)	106.9 (2)
Average	109.47	109.4	109.4	109.3	109.5
O3−H	0.805 (1)	0.754 (2)	0.762 (3)	0.758 (3)	0.767 (2)
O3−H···O1	2.976 (2)	2.893 (2)	2.913 (4)	2.891 (4)	2.914 (3)

* From Basciano and Peterson (2007)

refinement. The data refinement details and unit-cell dimensions are given in Table 6. The atomic coordinates and site occupancies are given in Table 7 and selected interatomic distances and angles are given in Table 8. Data for end-member hydronium jarosite is taken from Basciano and Peterson (2007).

There is a progressive change in unit-cell dimensions of the $(NH_4)_{1-x}(H_3O)_xFe_3(SO_4)_2(OH)_6$ solid-solution with increasing ammonium content. The unit-cell dimensions a vs. c are plotted in Fig. 4. The data plot close to a straight line with a correlation coefficient of $r^2 = 0.98$. There is no H_3O^+ substitution in the A site of end-member ammoniojarosite, causing the unit-cell dimension a to be smaller and c to be larger than for the synthetic ammoniojarosite samples grown by Dutrizac and Kaiman (1976) and Smith and Lampert (1973). The samples synthesized in these previous studies contain appreciable amounts of hydronium (9% and 20%, respectively) and plot between samples C and D from the current study. Unit-cell dimensions vs. ammonium content for the synthetic ammonium−hydronium jarosite series is shown in Fig. 5. With increasing ammonium content, unit-cell dimension a is reduced by a little and unit-cell dimension c undergoes a relatively large increase. As in other jarosite group members, substitution in the A site mainly affects unit-cell dimension c. End-member hydronium jarosite is non-stoichiometric with respect to hydronium due to A site occupancy of 92% (Basciano and Peterson, 2007). Unit-cell parameter c is smaller than expected as a result of the A-site deficiency.

The unit-cell dimensions of two natural ammoniojarosite samples are included in Fig. 4. Sample M16514 from Utah has similar unit-cell dimensions to those of the synthetic end-member ammonio-jarosite. Sample M38446 plots to the left of the synthetic samples from this study. It was determined with SEM-EDS analysis that the sample contains a minor amount of Al in the B site, which causes a reduction in unit-cell dimension a (Brophy et al., 1962). The sample has a similar c dimension to end-member ammoniojarosite, indicating that the A site is predominantly filled with ammonium with minor

hydronium substitution. No other cations were found (with SEM-EDS analysis) in either sample that would substitute into either the A or B site. Similar to findings by Basciano and Peterson (2007), natural samples of jarosite are often not B-site deficient due to slower growth conditions. Additionally, natural samples are usually close to end-member compositions or zoned. Based on unit-cell dimensions, both natural samples in this study are end-member ammoniojarosite with a small amount of hydronium substitution in the A site. Unit-cell dimensions can be used quite reliably to determine substitution in the A and B sites of jarosite samples (Basciano and Peterson, work in progress).

Polyhedral bond lengths A−O2 and O3 and Fe−O2 and O3 of the synthetic samples are shown in Fig. 6. Polyhedral bond lengths of the A and B site vary linearly according to occupancy. With ammonium substitution into hydronium jarosite, A−O3 increases and A−O2 decreases. Correspondingly, Fe−O3 remains relatively constant and Fe−O2 increases. The A−O2 bond distance for hydronium jarosite is smaller than the trend would indicate as a result of non-

stoichiometry of the A site with 92% H_3O occupancy (Basciano and Peterson, 2007). The difference in bond length between sample B (32% NH_4 occupancy) and sample E (100% NH_4 occupancy) is 0.046 Å. This is similar to the difference in the Fe−O2 bond lengths between samples B and E (0.049 Å). Substitutions in the A site mainly affect the Fe−O2 bond length. Substitution of NH_4 in the A site increases bond length A−O3 by 0.052 Å. The ionic diameter of H_3O^+ is 1.52 Å (Dutrizac and Jambor, 2000) and of NH_4^+ is 1.69 Å in 9-fold coordination (Khan and Baur, 1972). In 12-fold coordination the diameter of NH_4^+ is probably >1.69 Å (Altaner et al., 1988). Bond distances A−O3 and Fe−O2 are directed predominantly along the c axis. As NH_4^+ occupancy of the A site increases, its bonding contribution to O3 also increases. This is compensated by a slight increase in the Fe−O2 distance and an enlargement of the structure in the c direction by increasing A−O3 distances. As the O2···H2−N bond (A−O2) shortens, the H bonding contribution to O2 increases and is compensated by enlargement of the Fe−O2 and A−O3 bonds.
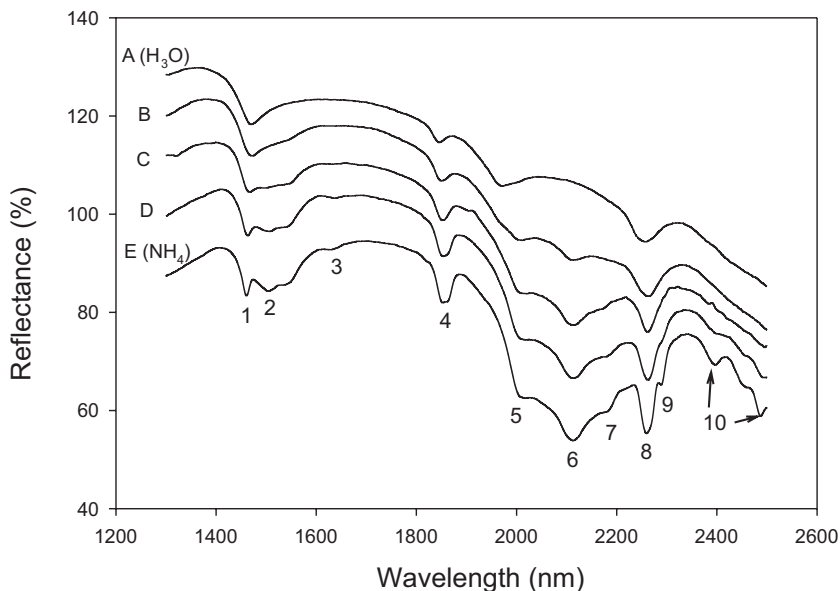

FIG. 7. SWIR spectra of samples from the NH_4−H_3O jarosite solid-solution series: NH_4 contents of samples B, C and D are 32, 59 and 93 at.%, respectively. Bands have been assigned to the following: 1 (1460 nm): OH vibration and H_2O absorption, 2 (1504 nm): Fe–OH vibration, 4 (1854 nm): Fe–OH vibration, 8 (2260 nm): Fe–OH vibration, 9 (2288 nm): Fe−OH vibration, and 10 (2396−2488 nm): $(SO_4)_2$ stretching and OH vibration. Bands labelled 3 (1634 nm), 5 (1990 nm), 6 (2112 nm) and 7 (2186 nm) are attributed to NH_4 (Altaner et al., 1988). Band assignments for 1, 2, 4, 8, 9 and 10 were taken from Bishop and Murad (2005). The spectra have been offset for comparison.
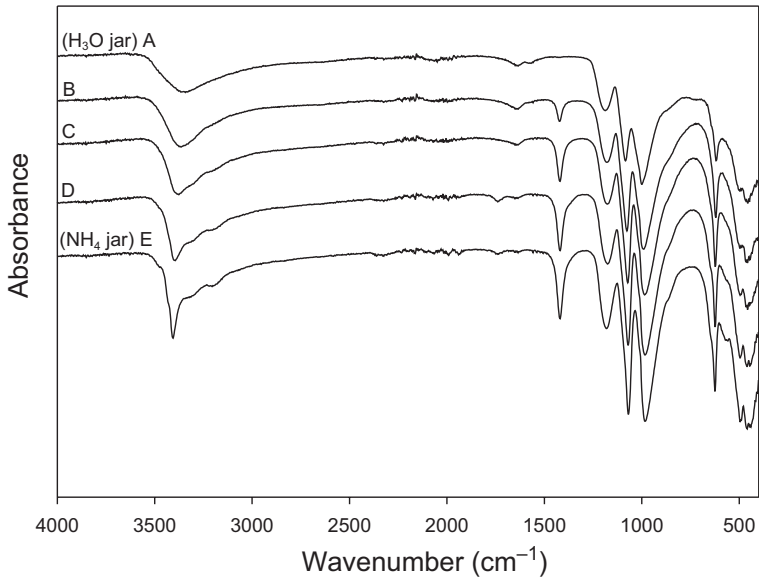
FIG. 8. FTIR spectra of samples from the NH_4-H_3O jarosite solid-solution series: NH_4 contents of samples B, C and D are 32, 59 and 93 at.%, respectively. Band assignments are given in Table 9. Note the band at 1423 cm^{-1}, attributed to $\nu_4(NH_4)$, can be a useful method of determining the approximate amount of ammonium substituting into the jarosite structure.

SWIR and FTIR

Short-wave infrared spectra for the synthetic NH_4-H_3O jarosite solid-solution series is shown in Fig. 7. Data for hydronium jarosite taken from Basciano and Peterson (2007) are included for completeness. The spectra are typical of the jarosite structure and the transmittance bands have been assigned based on the results of Bishop and Murad (2005). In the NH_4-H_3O jarosite solid-solution series there is a change in spectra which can be tracked across the sequence. The distinct SWIR patterns for ammoniojarosite, hydronium jarosite and Na/K jarosite (Basciano and Peterson, 2007) can enable rapid identification of the specific type of jarosite while in the field.

The FTIR spectra of ammoniojarosite have been discussed previously by Frost et al. (2006), Ristić et al. (2005) and Musić et al. (1993). The spectra obtained here are similar to those in the literature. The FTIR spectra for the ammoniojarosite−hydronium jarosite solid-solution series are shown in Fig. 8. Band assignments for vibrational features are given in Table 9. Hydronium in the *A* site is shown to cause peak shifts, peak widening (3407 cm^{-1}) and/or peak elimination. In particular, a sharp peak observed in ammoniojarosite and not hydronium jarosite occurs at 1423 cm^{-1}.

TABLE 9. Band assignments for vibrational features in synthetic ammoniojarosite and hydronium jarosite.

NH_4 jarosite	H_3O jarosite	Assignment
449	464 b	$\nu_2(SO_4)^{2-}$
464	−	Fe−O
495	503	Fe−O
573 sh	−	$\gamma(OH)$
624	623	$\nu_4(SO_4)^{2-}$
871 sh	−	$\delta(OH)$
987	1004	$\delta(OH)$
~1012 sh vw	−	$\delta(OH)$
1070	1089	$\nu_3(SO_4)^{2-}$
1184	1195	$\nu_3(SO_4)^{2-}$
1423	−	$\nu_4(NH_4)$
−	1576 sh	$\delta(H_2O)$
1647 vw	1639	$\delta(H_2O)$
1743	−	u.b.
3207	−	$\nu_3(NH_4)$
3320	−	$\nu_3(NH_4)$
3412	3367 b	$\nu(OH)$

sh = shoulder, b = wide, vw = very weak.
Band assignments are based on work by
Altaner et al. (1988), Bishop and Murad (2005) and
Frost et al. (2005).
u.b.: unidentified band

This peak is evident in sample B, which has 32% NH_4 occupancy and would probably be noted in samples with much less ammonium substitution, making it characteristic of ammonium-containing jarosite samples.

Acknowledgements

References

Altaner, S.P., Fitzpatrick, J.J., Krohn, M.D., Bethke, P.M., Hayba, D.O., Goss, J.A. and Brown, Z.A. (1988) Ammonium in alunites. *American Mineralogist*, **73**, 145−152.

Balzar, D. (1999) Voigt-function model in diffraction line-broadening analysis. *International Union of Crystallography Monographs on Crystallography*, **10**, 94−126.

Basciano, L.C. and Peterson, R.C. (2007) Jarosite−hydronium jarosite solid-solution series with full iron occupancy: mineralogy and crystal chemistry. *American Mineralogist*, **92**, 1464−1473.

Baur, W.H. (1972) Prediction of hydrogen bonds and hydrogen atom positions in crystalline solids. *Acta Crystallographica*, **B28**, 1456−1465.

Bishop, J.L. and Murad, E. (2005) The visible and infrared spectral properties of jarosite and alunite. *American Mineralogist*, **90**, 1100−1107.

Brophy, G.P., Scott, E.S. and Snellgrove, R.A. (1962) Sulfate studies II: Solid-solution between alunite and jarosite. *American Mineralogist*, **22**, 773−784.

Bruker, A.X.S. (2000) *Crystal structure analysis package, SHELXTL (Version 6.14), SAINT (Version 7.23A)*. Bruker AXS Inc., Madison, WI.

Cheary, R.W. and Coelho, A.A. (1998) Axial divergence in a conventional X-ray powder diffractometer I. Theoretical foundations. *Journal of Applied Crystallography*, **31**, 851−861.

Coelho, A.A. (2004) *TOPAS-Academic*. *http://members.optusnet.com.au/~alancoelho*.

Dowty, E. (2003) *ATOMS version 6.0*. Shape Software, Kingsport, Tennessee.

Drouet, C. and Navrotsky, A. (2003) Synthesis,

characterization, and thermochemistry of K-Na-H_3O jarosites. *Geochimica et Cosmochimica Acta*, **11**, 2063−2076.

Drouet, C., Pass, K.L., Baron, D., Draucker, S. and Navrotsky, A. (2004) Thermochemistry of jarosite-alunite and natrojarosite-natroalunite solid-solutions. *Geochimica et Cosmochimica Acta*, **68**, 2197−2205.

Dutrizac, J.E. and Kaiman, S. (1976) Synthesis and properties of jarosite-type compounds. *The Canadian Mineralogist*, **14**, 151−158.

Dutrizac, J.E. and Jambor, J.L. (2000) Jarosites and their application in hydrometallurgy. Pp. 405−452 in: *Sulfate Minerals − Crystallography, Geochemistry, and Environmental Significance* (C.N. Alpers, J.L. Jambor and D.K. Nordstrom, editors). Reviews in Mineralogy and Geochemistry, **40**. Mineralogical Society of America, Washington D.C.

Frost, R.L., Wills, R., Martens, W. and Weier, M. (2005) NIR spectroscopy of jarosites. *Spectrochimica Acta*, **A62**, 869−874.

Frost, R.L., Wills, R., Kloprogge, J.T. and Martens, W. (2006) Thermal decomposition of ammonium jarosite $(NH_4)Fe_3(SO_4)_2(OH)_6$. *Journal of Thermal Analysis and Calorimetry*, **84**, 489−496.

Glynn, P. (2000) Solid-solution solubilities and thermodynamics: Sulfates, carbonates, and halides. Pp. 481−511 in: *Sulfate Minerals: Crystallography, Geochemistry, and Environmental Significance* (C.N. Alpers, J.L. Jambor and D.K. Nordstrom, editors). Reviews in Mineralogy and Geochemistry, **40**. Mineralogical Society of America, Chantilly, Virginia.

Hendricks, S.B. (1937) The crystal structure of alunite and the jarosites. *American Mineralogist*, **22**, 773−784.

Hill, R.J. and Flack, H.D. (1987) The use of the Durbin-Watson *d* statistic in Rietveld analysis. *Journal of Applied Crystallography*, **20**, 356−361.

Hölzer, G., Fritsch, M., Deutsch, M., Härtwig, J. and Förster, E. (1997) $K\alpha_{1,2}$ and $K\beta_{1,3}$ X-ray emission lines of the 3^d transition metals. *Physical Review*, **A56**, 4554−4568.

Khan, A.A. and Baur, W.H. (1972) Salt hydrates: VIII. The crystal structures of sodium ammonium orthochromate dehydrate and magnesium diammonium bis (hydrogen orthophosphate) tetrahydrate and a discussion of the ammonium ion. *Acta Crystallographica*, **B28**, 683−693.

Kubisz, J. (1970) Studies on synthetic alkali-hydronium jarosites. I. Synthesis of jarosite and natrojarosite. *Mineralogia Polonica*, **1**, 47−57.

Majzlan, J., Stevens, R., Boerio-Goates, J., Woodfield, B.F., Navrotsky, A., Burns, P.C., Crawford, M.K. and Amos, T.G. (2004) Thermodynamic properties, low-temperature heat-capacity anomalies, and single-crystal X-ray refinement of hydronium jarosite,

$(H_3O)Fe_3(SO_4)_2(OH)_6$. *Physics and Chemistry of Minerals*, **31**, 518−531.

Musić, S., Popović, S., Orehovec, Z. and Czako-Nagy, I. (1993) Properties of precipitates formed by hydrolysis of Fe^{3+} ions in $NH_4Fe(SO_4)_2$ solutions. *Journal of Colloid and Interface Science*, **160**, 479−482.

Odem, J.K., Hauff, P.L. and Farrow, R.A. (1982) A new occurrence of ammoniojarosite in Buffalo, Wyoming. *The Canadian Mineralogist*, **20**, 91−95.

Ripmeester, J.A., Ratcliff, C.I., Dutrizac, J.E. and Jambor, J.L. (1986) Hydronium ion in the alunite-jarosite group. *The Canadian Mineralogist*, **24**, 435−447.

Ristić, M., Musić, S. and Orehovec, Z. (2005) Thermal decomposition of synthetic ammonium jarosite. *Journal of Molecular Structure*, **744−747**, 295−300.

Salinas, E., Roca, A., Cruells, M., Patino, F. and Córdoba, D.A. (2001) Characterization of alkaline decomposition − cyanidation kinetics of industrial ammonium jarosite in NaOH media. *Hydrometallurgy*, **60**, 237−246.

Scott, K.M. (1987) Solid-solution in, and classification of, gossan-derived members of the alunite-jarosite family, northwest Queensland, Australia. *American Mineralogist*, **72**, 178−187.

Shannon, E.V. (1927) Ammoniojarosite, a new mineral of the jarosite group from Utah. *American Mineralogist*, **12**, 424−426.

Shannon, E.V. (1929) Tschermigite, ammoniojarosite, epsomite, celestite, and paligorskite from southern Utah. *U.S. National Museum Proceedings*, **74**, 1−13.

Smith, W.L. and Lampert, J.E. (1973) Crystal data for ammoniojarosite $NH_4Fe_3(OH)_6(SO_4)_2$. *Journal of Applied Crystallography*, **6**, 490−491.

Stoffregen, R.E. (1993) Stability relations of jarosite and natrojarosite at 150−250ºC. *Geochimica et Cosmochimica Acta*, **57**, 2417−2429.

Stoffregen, R.E. and Alpers, C.N. (1987) Woodhouseite and svanbergite in hydrothermal ore deposits: Products of apatite destruction during advanced argillic alteration. *The Canadian Mineralogist*, **25**, 201−211.

Young, R.A. (1993) Introduction to the Rietveld method. Pp. 1−38 in: *The Rietveld Method* (R.A. Young, editor). Oxford Science Publications, UK.